

## Ultra-long Nanorods of Single-crystalline $\text{Na}_{0.44}\text{MnO}_2$ as Cathode Materials for Sodium-ion Batteries

Rui Ma, Handong Jiao, Hongmin Zhu, Shuqiang Jiao\*

State Key Laboratory of Advanced Metallurgy, School of Metallurgical and Ecological Engineering, University of Science and Technology Beijing, Beijing 100083, PR China

\*E-mail: [sjiao@ustb.edu.cn](mailto:sjiao@ustb.edu.cn)

Received: 22 May 2016 / Accepted: 19 June 2016 / Published: 7 July 2016

---

Rechargeable batteries composed of low-cost and abundant materials operating at room temperature are attractive for grid-scale energy storage application. Sodium-ion battery is thought of as an ideal candidate for secondary battery. Hence, ultra-long nanorods of single-crystalline  $\text{Na}_{0.44}\text{MnO}_2$  have been synthesized by co-precipitation method followed by high-temperature calcination. The obtained powder is pure phase with an orthorhombic lattice structure and the morphology is regular. Their electrochemical properties were thoroughly investigated in assembled Sodium-ion cells using cyclic voltammetry, galvanostatic testing, and electrochemical impedance spectroscopy. With applying the as-prepared  $\text{Na}_{0.44}\text{MnO}_2$  as a cathode material for sodium-ion batteries, it exhibits a high reversible initial capacity of  $94.1 \text{ mAh g}^{-1}$  in a voltage range of 2.0-4.0 V vs.  $\text{Na}^+/\text{Na}$  at a current density of  $50 \text{ mA g}^{-1}$ , and a satisfactory cyclability of 93.3% capacity retention after 200 cycles is performed in our work. The single-crystalline  $\text{Na}_{0.44}\text{MnO}_2$  with an excellent electrochemical performance proves that it is a potential cathode material for sodium-ion battery.

---

**Keywords:**  $\text{Na}_{0.44}\text{MnO}_2$ , single-crystalline, co-precipitation method, cathode materials

### 1. INTRODUCTION

The increasing concerns about the exploitations of fossil fuel have created a great demand for renewable energy resources. With the imminent exhaustion of fossil fuel resources and rising environmental problems, a variety of renewable and clean energy sources, such as tidal, wave, wind and solar power, are growing rapidly[1, 2]. Lithium-ion batteries (LIB) are considered one of the most attractive technologies for rechargeable energy storage for electric vehicles (EVs) and Hybrid Electric Vehicles (HEVs) because of their largest energy density and long cycle life[3-6]. Compared with Lithium-ion batteries, Sodium-ion batteries are much cheaper owing to the abundance availability in

the earth and the low cost of sodium, which makes Na-ion batteries show great potential to apply to large scale energy storage devices[7]. Recent years, a good deal of academic interest in Na-ion batteries has been focused on the development of cathode materials.

The main challenge in advancing Na-ion batteries technology lies in exploring outstanding electrode materials. Important battery performance characteristics such as specific capacity and redox potential are mainly determined by the electrochemical properties of the electrode materials. It is essential to discover new high-capacity sodium-based energy storage materials or to improve the known sodium compounds suitable for Na-ion batteries. The sodium manganese oxides such as  $\text{NaMnO}_2$ ,  $\text{Na}_{0.67}\text{MnO}_2$ ,  $\text{Na}_{0.44}\text{MnO}_2$  and other Na compounds ( $\text{Na}_x\text{Mn}_y\text{A}_z\text{O}_2$ , A=transition metal) have been regarded as promising cathode materials due to their high capacity, low cost and non-toxicity[8-12]. Among various cathode materials for sodium ions,  $\text{Na}_{0.44}\text{MnO}_2$  is identified as one of the most promising Na-ion batteries cathode materials because of its large capacity (theoretically  $121 \text{ mAh g}^{-1}$ ) and good stability[13].

The wide S-shaped tunnels in the orthorhombic structure are suitable for inserting/extracting the relatively large  $\text{Na}^+$  (compared to  $\text{Li}^+$ )[14, 15] during charging/discharging process in Na-ion batteries[16, 17].  $\text{Na}_{0.44}\text{MnO}_2$  can be synthesized via various approaches such as solid-state approach[18-20], glycine-nitrate combustion,<sup>21</sup> hydrothermal synthesis[22, 23], thermo-chemical conversion[24], polymer-pyrolysis<sup>14</sup>, molten salt synthesis[25] and reverse microemulsion method[26]. However, the solid-state reaction approach as discussed above has poor dispersion unregular shape morphology and large particle size, affecting battery performance. A co-precipitation technique is always applied to prepare the electrode material, which is cheap and easy to obtain the target compound. Hence, in this work, the co-precipitation technique has been adopted to prepare the  $\text{Na}_{0.44}\text{MnO}_2$  materials, which is not only directly to get uniform chemical composition by means of various chemical reactions in solution, but also easily to prepare materials with small particle size and well-distribution. The cathode material has showed an excellent electrochemical performance with high and stably cyclized capability through electrochemical measurements. The  $\text{Na}_{0.44}\text{MnO}_2$  through co-precipitation method proves that it is a potential cathode material for sodium-ion battery.

## 2. EXPERIMENTAL SECTION

*Synthesis of the  $\text{Na}_{0.44}\text{MnO}_2$ .* - All reagents and chemicals were purchased commercially and used as received. Single crystalline  $\text{Na}_{0.44}\text{MnO}_2$  material was prepared with a co-precipitation method using sodium hydroxide and manganese nitrate as the starting materials. Two aqueous solutions, namely, 1 mol/L sodium hydroxide solution and 1 mol/L manganese nitrate solution, were prepared. And then, oxygen was bubbled into the continuously agitated manganese nitrate solution. After oxidation of long time, a sodium hydroxide solution was added to a manganese nitrate solution by drop to form a mixture in which the stoichiometric molar ratio of sodium ions to manganese ions was up to 0.44:1. After co-precipitation reaction of 12h, the colloid mixture was dried to vapor the water in  $100^\circ\text{C}$  in air and then the black precursor was obtained. The black precursor was dried subsequently calcined at 650, 750 850  $^\circ\text{C}$  for 24h in air.

*Characterization* -The morphology and microstructure of the as-prepared  $\text{Na}_{0.44}\text{MnO}_2$  were characterized by X-ray diffraction (XRD, Rigaku, D/max-RB) with a Cu  $K\alpha_1$  radiation at  $\lambda=1.54 \text{ \AA}$ , field emission scanning electron microscopy (FESEM, JEOL, JSM-6701F), transmission electron microscopy (TEM, JEOL, JEM-2010) and high resolution Raman spectrometry (Horiba-labram HR evolution) with an excitation at 532 nm. X-ray photoelectron spectroscopy (XPS, Kratos AXIS Ultra DLD) was also applied to study the change of the valence state.

*Electrochemical Measurements.* -The cathode  $\text{Na}_{0.44}\text{MnO}_2$  was prepared by mixing 75 wt%  $\text{Na}_{0.44}\text{MnO}_2$  powder as the active material, 15 wt% acetylene carbon black conductive additive, and 10 wt% Teflon [poly(tetrafluoroethylene), PTFE] binder dissolved in anhydrous ethyl alcohol which worked as a solvent, to form a slurry. Then, the slurry was casted uniformly on aluminum foil and dried at  $100^\circ\text{C}$  in air for 12h to remove the residual solvent. The electrode material loading was about  $2 \text{ mg cm}^{-2}$ . Electrochemical tests of the electrode materials were measured by means of coin-type cell CR2032 in which the  $\text{Na}_{0.44}\text{MnO}_2$  cathode was used as working electrode and sodium metal was used as counter and reference electrodes. The electrolyte was  $1 \text{ mol L}^{-1}$   $\text{NaClO}_4$  dissolved in propylene carbonate (PC), and the separator was a glass fiber (GF/D). The coin cells were assembled in an argon-filled glovebox. The galvanostatic charge and discharge test was conducted at a voltage interval of 2.0 to 4.0 V (vs.  $\text{Na}^+/\text{Na}$ ) with a Neware BTS-53 tester. Cyclic voltammetry (CV, CHI1140A) measurements were also carried out with the coin cell at a scan rate of  $0.1 \text{ mV s}^{-1}$  between 2.0 and 4.0 V vs.  $\text{Na}^+/\text{Na}$ . To obtain the diffusion coefficient of sodium ions within the  $\text{Na}_{0.44}\text{MnO}_2$  cathode, electrochemical impedance spectroscopy measurements were carried out with a frequency response analyzer (EIS, CHI 1140A) in the frequency range of 100 kHz to 0.1 Hz. X-ray photoelectron spectroscopy (XPS, Kratos AXIS Ultra DLD) was performed on a Kratos AXIS Ultra DLD with monochromatic Al  $K\alpha$  ( $h\nu = 1486.6 \text{ eV}$ ). All XPS spectra were corrected according to the C 1s spectrum at 284.8 eV. Curve fitting and background subtraction were accomplished using XPSPEAK software.

### 3. RESULTS AND DISCUSSION

$\text{Na}_{0.44}\text{MnO}_2$  is isostructural with  $\text{Na}_4\text{Mn}_4\text{Ti}_5\text{O}_{18}$  and crystallizes in an orthorhombic system structure (*Pbam* space group). Fig.1a schematically shows that the framework of  $\text{Na}_{0.44}\text{MnO}_2$  is made up of  $\text{MnO}_5$  pyramids and  $\text{MnO}_6$  octahedra which are arranged to form two types of tunnels: large S-shaped tunnels and smaller pentagon tunnels.

These two kinds of polyhedra are interconnected by sharing corners to form two types of two unique tunnels as reported in previous work[26]. All  $\text{Mn}^{4+}$  ions and half of the  $\text{Mn}^{3+}$  ions are in octahedral sites, while the other  $\text{Mn}^{3+}$  ions are gathered in a pyramidal environment.  $\text{Na}1$  sites are located in the smaller tunnels while  $\text{Na}2$  and  $\text{Na}3$  are located in the large S-shaped tunnels. According to the framework, these tunnels serve as diffusion paths for free transport of sodium ions, mainly along the c-axis direction. Sodium ions in the large S-shaped tunnels are considered to be move and can potentially be reversibly extracted while the sodium ions in the small tunnels cannot be extracted.

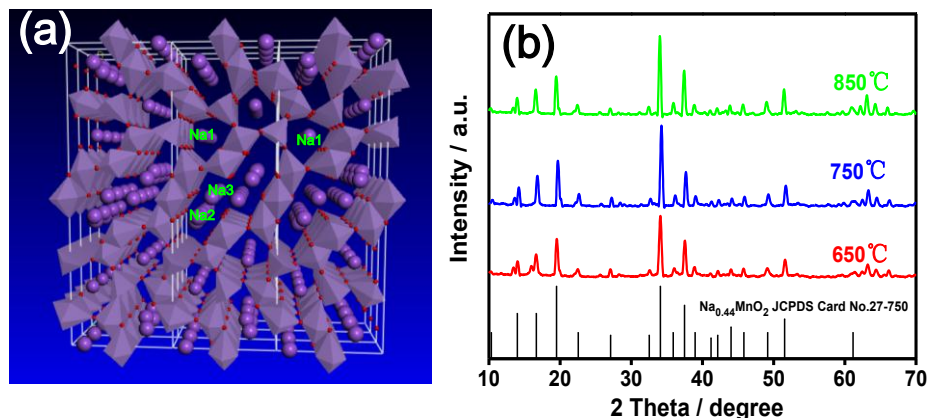


**Figure 1.** (a) Schematic crystal structure of orthorhombic of  $\text{Na}_{0.44}\text{MnO}_2$  (looking down the c-axis). (b) XRD pattern of as-prepared  $\text{Na}_{0.44}\text{MnO}_2$  materials calcined at different temperatures.

The synthesized powder  $\text{Na}_{0.44}\text{MnO}_2$  was synthesized using a co-precipitation method. The XRD pattern in Fig.1b shows that the prepared  $\text{Na}_{0.44}\text{MnO}_2$  material crystallizes well in standard pattern of the orthorhombic  $\text{Na}_{0.44}\text{MnO}_2$  phase (PDF card no.27-0750). No impurities such as  $\text{Mn}_2\text{O}_3$  and  $\text{Mn}_3\text{O}_4$  phases, were detectable in all the XRD patterns from 650 to 850 °C, in which the five strongest peaks located at 14.1°, 16.7°, 19.6°, 34.2°, and 37.5° correspond to the (130), (140), (200), (350), and (201) plane reflections, respectively, indicating that the co-precipitation reaction is an effective prepare method for  $\text{Na}_{0.44}\text{MnO}_2$ . In particular, it is found that sample synthesized at 750°C has the low impurity content and high crystallinity.

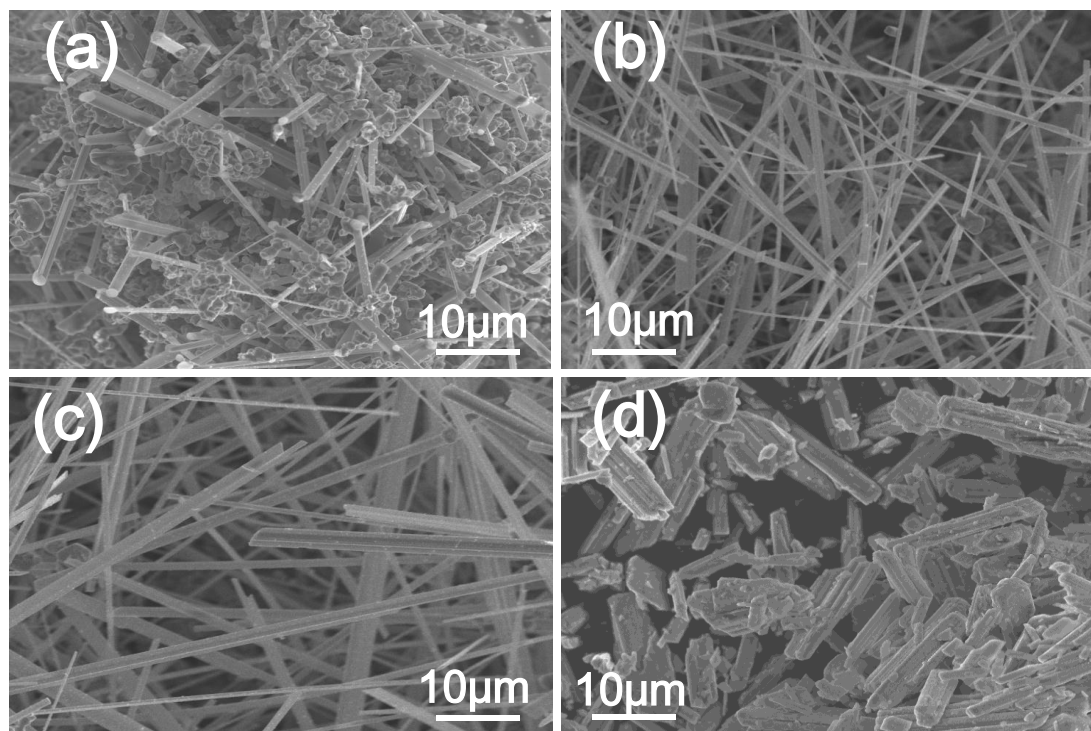


**Figure 2.** SEM images of  $\text{Na}_{0.44}\text{MnO}_2$  heat-treatment at (a) 450, (b) 650, (c) 750 and (d) 850 °C

The synthesized powder are well crystallized, as is observed with the Fig.2, and have grown anisotropically, leading to rod shapes. It is clear that from Fig.2a, at 450 °C, the materials appear to be quite disordered and most of the graininess morphologies are mingled with a few nanorod-like structures, showing poor crystallization at low temperatures.

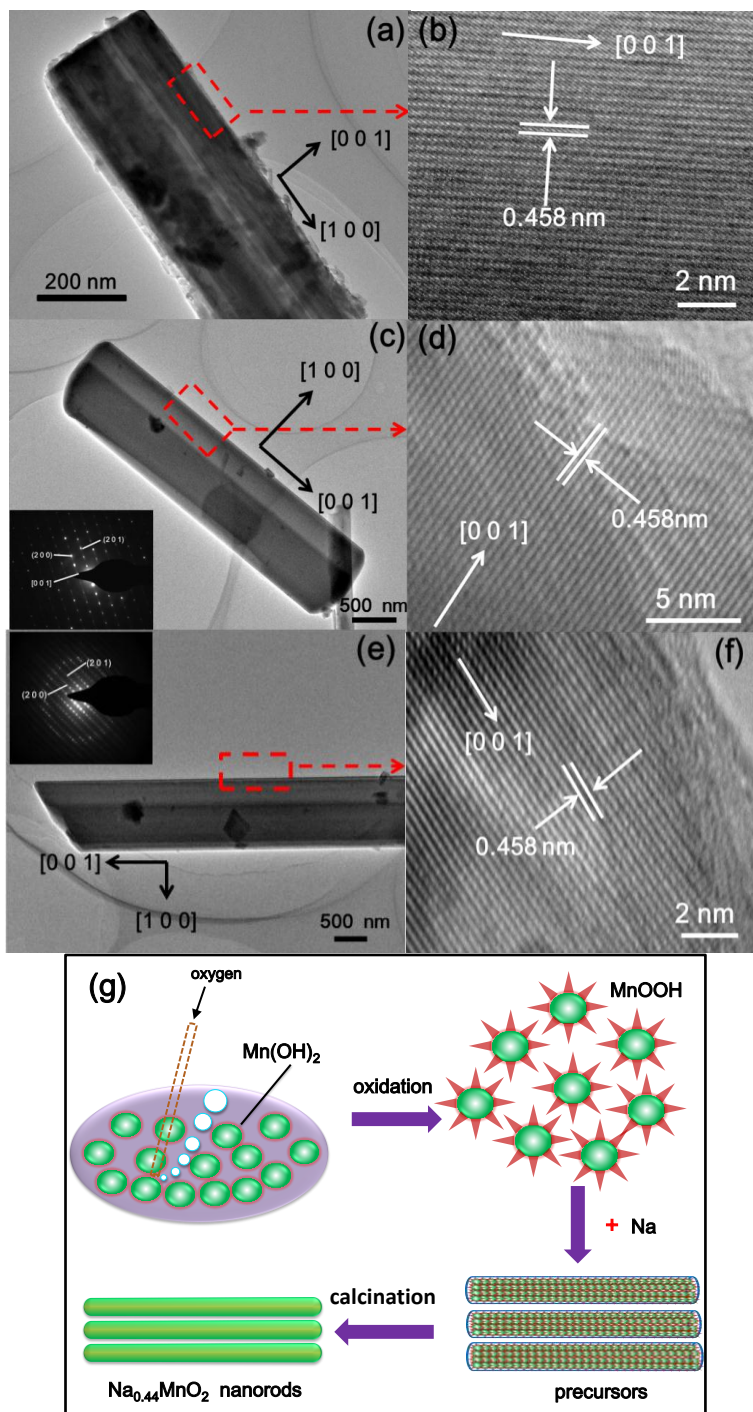


**Figure 3.** TEM images of Na<sub>0.44</sub>MnO<sub>2</sub> heat-treatment at (a) 650, (c) 750 (insert of SAED) (e) 850°C (insert of SAED). HRTEM images of Na<sub>0.44</sub>MnO<sub>2</sub> heated at (b) 650, (d) 750 (f) 850°C. (g) Schematic illustration of synthesis method of single single-crystalline Na<sub>0.44</sub>MnO<sub>2</sub>.

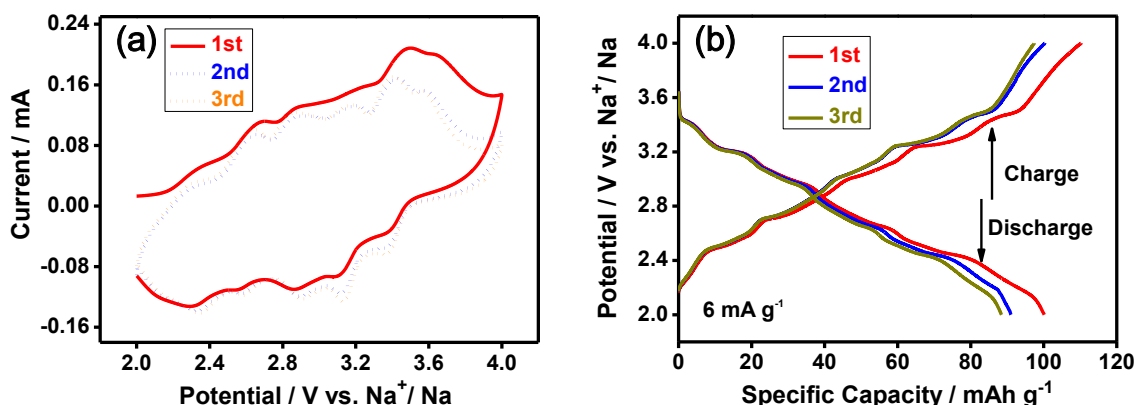
A large majority of nanorod structures which are uniform and well-distributed, begin to appear after 650 °C heat-treatment (Fig.2b). When the annealing temperature was further increased to 750 °C (Fig. 2c), the average size of ultra-long nanorods was further enlarged (length > 10 μm; 0.5~4 μm in width). As seen from this image, the Na<sub>0.44</sub>MnO<sub>2</sub> nanorods have higher crystallinity. The SEM image of the 850 °C in Fig.2d indicates that at high temperature, micro-morphology of Na<sub>0.44</sub>MnO<sub>2</sub> are irregular shape and the nanorods start to adhere together and become thicker even shrunken, compared with the appearance of 750 °C. Moreover, many fragments disperse around the bar-shaped nanorod. The phenomenon, the particle size increases with the rise of sintering temperature, is basically ascribed to the high temperature contributes to the crystal particle growth of materials.

Fig.3 exhibits the TEM images of the as-prepared Na<sub>0.44</sub>MnO<sub>2</sub>, sintered at 650°C, 750°C and 850°C. It can be seen that the materials heat-treatment at different temperatures display nanorod-like morphologies with different diameter sizes, while they display similar nanorod-like crystallite morphology. TEM images of the Na<sub>0.44</sub>MnO<sub>2</sub> sample treated at 650 °C display thin nanorod morphology with a diameter size of ~210 nm (Fig.3a), but many cavities are observed inside the nanorods, indicating incomplete crystallization and a high density of defects.

The high-resolution TEM image in Fig. 3b shows the crystalline phase and the nanorod growth direction is along the [001] orientation, which is coordination with previous reports[14]. The rate of crystal growth of crystal plane along [001] direction is faster than along other directions. The crystallization turns better at 750°C (Fig.3c), but the bigger diameter size of rod can be noticed from the image. The interplanar distance is about 0.46 nm, which is corresponding to (200) lattice plane, indicating the growth direction is parallel to the (200) lattice plane. A selected area electron diffraction (SAED) pattern (insert of Fig.3c) reveals that the nanorods are single-crystalline structure. Fig.3d shows that implying a good crystallization at a relatively high temperature(750 °C). The diameter(~1.2 μm) of the sample sintered at 850 °C is larger than that heated at 650 and 750 °C, according to Fig.2e. The corresponding SAED pattern shows diffraction spots with roughly high symmetry, and the crystal lattice of regular arrangement, indicating the as-prepared rod-like Na<sub>0.44</sub>MnO<sub>2</sub> is single-crystalline (Fig. 3e). From what has been discussed above, all of the results are in agreement with the SEM and TEM images. Based on the results mentioned above, the formation process of Na<sub>0.44</sub>MnO<sub>2</sub> nanorods can be expressed by Fig. 3g. A brown Mn(OH)<sub>2</sub> hydroxide suspension is oxidized into MnOOH, and then the Na substituted a portion of OH to form a sodium birnessite compound(precursor)[27, 28]. Finally, the obtained black gel precursors are sintered at high temperature in order to remove superfluous hydroxide compound. In this way, a regular and uniform morphology is obtained.

Sodium ions insertion/extraction properties of the Na<sub>0.44</sub>MnO<sub>2</sub> samples treated at high temperature were investigated by cyclic voltammetry (CV) and galvanostatic charge/discharge cycling. Fig 4a shows typical CV curves of a nanorod Na<sub>0.44</sub>MnO<sub>2</sub> electrode treated at 750 °C. The three obvious oxidation peaks in the initial CV scan are stronger than those in the subsequent scans, revealing some degree of irreversible reactions of sodium ion extraction from the substrate. The initial irreversible phenomenon likely originates from initial multiatomic transition processes to accommodate the structural strain for sodium ion insertion/extraction, and from the surface reaction between electrolyte and electrode[20]. After the first scan, the subsequent CV curves exhibit at least six pairs of quite symmetrical redox peaks, implying a complex multiphase transition mechanism

during sodium ion insertion and extraction processes[20]. But significant changes cannot be observed for the reduction peaks during the initial three cycles, demonstrating that the discharge process is stable, in which sodium ion insertion behavior is reversible.

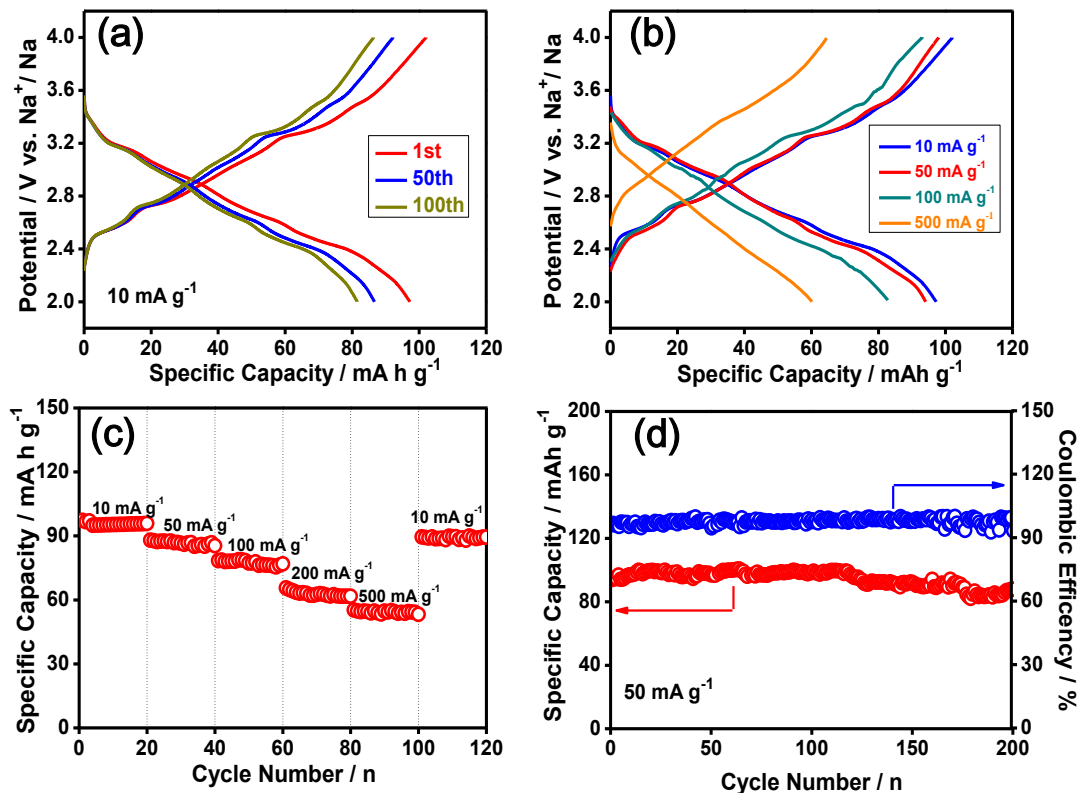


**Figure 4.** (a) The initial three cyclic voltammetry profiles of Na<sub>0.44</sub>MnO<sub>2</sub> sintered at 750 °C at the scan rate of 0.1 mV s<sup>-1</sup> in the voltage range of 2.0 to 4.0 V (vs. Na<sup>+</sup>/Na). (b) The galvanostatic charge and discharge profiles of Na<sub>0.44</sub>MnO<sub>2</sub> calcined at 750 °C tested in the voltage range of 2.0 to 4.0 V (vs. Na<sup>+</sup>/Na) at a constant current of 6 mA g<sup>-1</sup> (0.05 C).

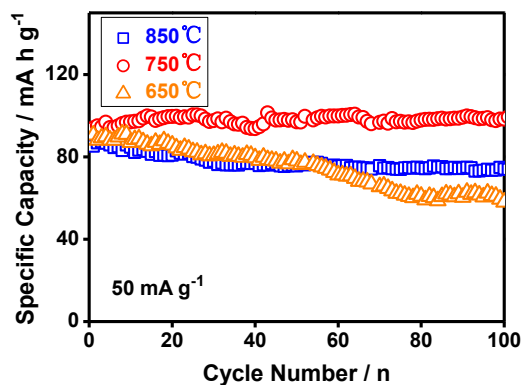
The first three galvanostatic charge and discharge cycles of Na<sub>0.44</sub>MnO<sub>2</sub> calcined at 750 °C tested in the voltage range of 2.0 to 4.0 V at a constant current of 6 mA g<sup>-1</sup> (0.05 C, C=121 mA g<sup>-1</sup>), is shown in Fig.4b. The sampling cathode exhibits initial charge and discharge specific capacity of 110.2 and 100.1 mAh g<sup>-1</sup>, respectively. The first cycle irreversible capacity loss can be seen from the charge and discharge curves, which is corresponding to the stronger oxidation peak during the first CV scan. Many voltage plateaus are distinctly observed in the charge and discharge curves, in good agreement with the CV measurements.

Fig. 5a shows the initial 100 cycle charge and discharge curves of Na<sub>0.44</sub>MnO<sub>2</sub> electrodes at a current density of 10 mA g<sup>-1</sup>. It is found that the first cycle has charge and discharge capacities of 102.2 mA h g<sup>-1</sup> and 97.0 mA h g<sup>-1</sup>, respectively. The initial charge and discharge curves of Na<sub>0.44</sub>MnO<sub>2</sub> nanorods at different current densities from 10 to 500 mA g<sup>-1</sup> are shown in Fig. 5b. With the increase of the current density, the specific capacity declines. It should be emphasized that the as-prepared sample is capable of reversibly intercalating sodium-ions and exhibits good rate performance. Even at a high current of 500 mA g<sup>-1</sup>, the charge and discharge capacities can remain at 64.5 and 60.1 mA h g<sup>-1</sup>, respectively. Cycling performance of the Na<sub>0.44</sub>MnO<sub>2</sub> electrode at current densities from 10 to 500 mA g<sup>-1</sup> is illustrated by Fig. 5c. The electrode material exhibits good cyclability within the first 120 cycles, and the discharge specific capacity almost go back to the initial capacity when the discharge current density returns to 10 mA g<sup>-1</sup> from 500 mA g<sup>-1</sup>, indicating that, the intercalation/extraction of Na ions for the Na<sub>0.44</sub>MnO<sub>2</sub> electrode is reversible even at high current densities. The high cyclability is a result of no structures evidenced via in-situ XRD measure and the formation of highly crystalline

structures<sup>20</sup>. To the best of our knowledge, this material exhibits splendid performance in terms of high capacity and excellent cycling stability for sodium-ion battery.



**Figure 5.** The electrochemical performance of Na<sub>0.44</sub>MnO<sub>2</sub> electrode. (a) The initial 100 cycle charge and discharge curves at a current of 10 mA g<sup>-1</sup>. (b) The initial charge and discharge curves at different current densities. (c) Discharge capacity of Na<sub>0.44</sub>MnO<sub>2</sub> rods calcined at 750 °C as a function of charge and discharge cycles at different charge/discharge current densities of 10, 50, 100, 200, 500 mA g<sup>-1</sup>. (d) The cycling performance and coulombic efficiency at a current of 50 mA g<sup>-1</sup>.



**Figure 6.** Cycle performance of Na<sub>0.44</sub>MnO<sub>2</sub> samples sintered at 650, 750, and 850 °C at a current density of 50 mA g<sup>-1</sup>.

From what has been discussed above, we can learn that the micro-morphology of material is influenced by different sintering temperature. In Fig. 6, it shows the cycling performance of the treated at different temperatures. In detail, the  $\text{Na}_{0.44}\text{MnO}_2$  calcined at 650 and 850 °C retained capacity of 60.1 and 74.1  $\text{mAh g}^{-1}$  after 100 cycles, corresponding to 66.7% and 87.1% capacity retention of their initial capacity. In sharp contrast, the sample treated at 750 °C demonstrated excellent cyclic stability. The discharge capacity remained 98.4  $\text{mAh g}^{-1}$  after 100 cycles at the current density of 50  $\text{mA g}^{-1}$ , even 93.4% capacity retention of their initial capacity after 200 cycles. The better cycling performance at 750 °C is because of the suitable particle size of the sample, which can contribute to the diffusion of sodium ions in the bulk of the electrode. The particle size grows bigger when sintered at 850 °C, leading to more stress during the sodium ions insertion and extraction. At lower temperatures, unstable capacity retention during battery charging/discharging results from poor crystallization.

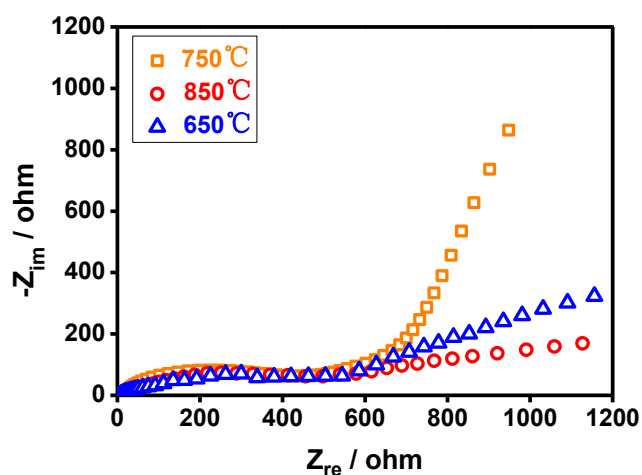


**Figure 7.** Typical Nyquist plots obtained for  $\text{Na}_{0.44}\text{MnO}_2$  cell over the frequency range from 100 kHz to 0.1 Hz.

The electrical conductivity of  $\text{Na}_{0.44}\text{MnO}_2$  was investigated using the AC impedance technique at various temperatures. Fig. 7 shows the typical Nyquist plots obtained at various temperatures for the cell and each of the impedance spectra consists of a depressed semicircle at high frequency, then followed by a straight sloping line in the low frequency range. The semicircle part at high frequency region is associated with the charge transfer process at the electrode–electrolyte interface. In the case of the diffusion impedance, the sloping line in the low frequency region deviates from the Warburg impedance, which is attributed to the diffusion behavior of sodium ions in the bulk of the electrode. Compared with  $\text{Na}_{0.44}\text{MnO}_2$  calcined at 700 and 800 °C, the sample sintered at 750 °C exhibits the lowest Warburg impedance, which implies that the diffusion of sodium ions in the bulk of the material is faster.

X-ray photoelectron spectroscopy (XPS), a useful tool to understand the oxidation state of the Mn element, was employed for the investigating extraction and intercalation of sodium ions during the charging and discharging progress. All the electrode materials for testing the spectra were essentially

prepared at same requirements. An XPS spectrum of the  $\text{Na}_{0.44}\text{MnO}_2$  powder in the binding energy range of 800 to 500 eV is illustrated in the Fig. 8a, where typical Mn  $2p^{1/2}$  and Mn  $2p^{3/2}$  spectra in the red dotted line circle were conducted in the research.

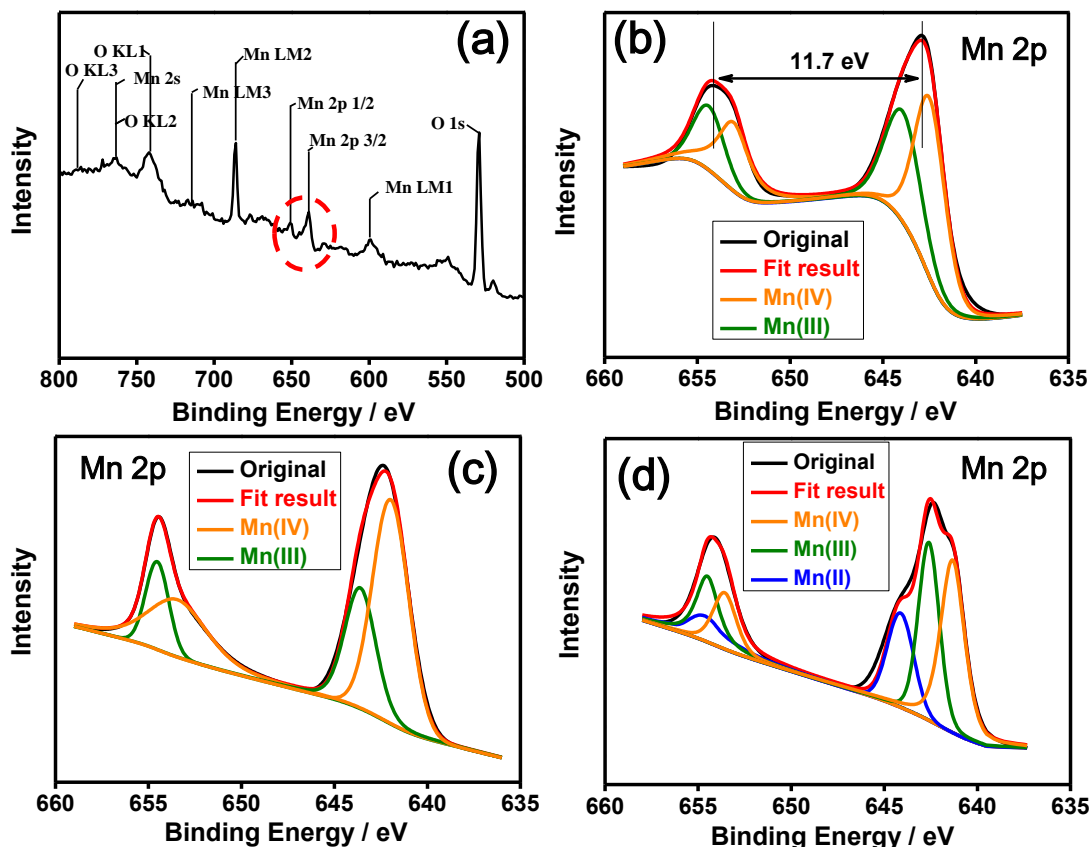


**Figure 8.** XPS spectra of (a) the as-prepared  $\text{Na}_{0.44}\text{MnO}_2$  in the binding energy range of 800 to 500 eV and (b) Mn 2p branch. XPS spectra of the cathode after (c) a fully charge process to 4.0 V and (d) a fully discharge process to 2.0 V respectively.

To observe the differences between the as-prepared electrodes before and after galvanostatic charge-discharge, high resolution Mn 2p photoelectron spectra of the  $\text{Na}_{0.44}\text{MnO}_2$  can clearly be seen from the Fig. 8b, in which the distinct peaks at  $\sim 653.8$  and  $\sim 642.1$  eV were assigned to the Mn  $2p^{1/2}$  and Mn  $2p^{3/2}$  XPS peaks, respectively, with a spin-orbit energy splitting of 11.7 eV[22, 29]. The Mn 2p spectrum before battery measures can be divided into two major components, corresponding to Mn (IV) and Mn (III) with a mole ratio of 46%: 54%. During discharging progress, oxidation state of the Mn cations will increase due to intercalation of sodium ions. Upon fitting the spectrum, a consistent result that the amounts of Mn (IV) increases to 67% while the amount of Mn (III) decrease to 33%, was obtained which is shown in Fig. 8c. However, after charge, the fit spectrum appears another Mn (II) part[30], but 43% Mn (IV) and 35% Mn (III) can still be identified. It can be seen in Fig. 8d that oxidation state of the Mn cations decline because of sodium ions insertion into the cathode.

The XPS result is in good agreement with the electrochemical progress of  $\text{Na}_{0.44}\text{MnO}_2$  electrode, and provides more information to understand transportation of sodium ions in the bulk of cathode.

#### 4. CONCLUSIONS

In summary, tunnel-structured sodium manganese oxides  $\text{Na}_{0.44}\text{MnO}_2$  were prepared successfully by a co-precipitation reaction, which is not found in previous research reports.  $\text{Na}_{0.44}\text{MnO}_2$  cathode shows excellent electrochemical performance and higher cyclized capability is displayed in our research compared with other works[18, 22, 26]. Single-crystalline  $\text{Na}_{0.44}\text{MnO}_2$  displayed regular rod-shape morphology. Significantly, at a current density of  $50 \text{ mA g}^{-1}$ , the discharge capacity at the 1st and 200th cycle are 94.1 and  $87.8 \text{ mAh g}^{-1}$ , respectively. In particular, the sample electrode reveals a considerable coulombic efficiency of 99% at the 200th cycle. It is concluded that the  $\text{Na}_{0.44}\text{MnO}_2$  is a suitable material to store sodium ions and at the same time, the special structure and morphology of the sample improve their electrochemical properties. All the results suggest that  $\text{Na}_{0.44}\text{MnO}_2$  is a promising cathode material for sodium-ion batteries.

#### ACKNOWLEDGMENTS

This work was supported by the Fundamental Research Funds for the Central Universities (FRF-TP-15-002C1) and the National Natural Science Foundation of China (No 81301345).

#### References

1. H. Pan, Y. Hu, and L. Chen, *Energy Environ. Sci.*, 6 (2013) 2338.
2. Z. Yang, J. Zhang, M. C. Kintner-Meyer, X. Lu, D. Choi, J. P. Lemmon, and J. Liu, *Chem. Rev.*, 111 (2011) 3577.
3. J. M. Tarascon, N. Reham, M. Armand, J. N. Chotard, P. Barpanda, W. Walker, and L. Dupont, *Chem. Mater.*, 22 (2009) 724.
4. J. M. Tarascon, and M. Armand, *Nature*, 414 (2001) 359.
5. M. Armand, and J. M. Tarascon, *Nature*, 451 (2008) 652.
6. M. R. Palacin, *Chem. Soc. Rev.*, 38 (2009) 2565.
7. S. W. Kim, D. H. Seo, X. Ma, G. Ceder, and K. Kang, *Adv. Energy Mater.*, 2 (2012) 710.
8. J. P. Parant, R. Olazcuaga, M. Devalette, C. Fouassier, and P. Hagenmuller, *J. Solid State Chem.*, 3 (1971) 1.
9. D. Yuan, W. He, F. Pei, F. Wu, Y. Wu, J. Qian, Y. Cao, X. Ai, and H. Yang, *J. Mater. Chem. A*, 1 (2013) 3895.
10. J. Xu, D. Lee, R. J. Clement, X. Yu, M. Leskes, A. J. Pell, G. Pintacuda, X. Q. Yang, C. P. Grey, and Y. S. Meng, *Chem. Mater.*, 26 (2014) 1260.
11. K. Kubota, H. Yoshida, N. Yabuuchi, I. Ikeuchi, A. Garsuch, M. Schulz-Dobrick, and S. Komaba, *Electrochem. Soc.*, 2 (2014) 232.
12. D. Yuan, X. Hu, J. Qian, F. Pei, F. Wu, R. Mao, X. Ai, H. Yang and Y. Cao, *Electrochim. Acta*, 116 (2014) 300.
13. H. Zhu, K. T. Lee, G. T. Hitz, X. Han, Y. Li, J. Wan, S. Lacey, A. von Wald Cresce, K. Xu, E. Wachsman and L. Hu, *ACS Appl. Mater. Interfaces*, 6 (2014) 4242.
14. Y. Cao, L. Xiao, W. Wang, D. Choi, Z. Nie, J. Yu, Z. Yang and J. Liu, *Adv. Mater.*, 23 (2011) 3155.

15. V. Palomares, P. Serras, I. Villaluenga, K. B. Hueso, J. Carretero-González, and T. Rojo, *Energy Environ. Sci.*, 5 (2012) 5884.
16. L. Chen, Q. Gu, X. Zhou, S. Lee, Y. Xia, and Z. Liu, *Sci. Rep.*, 3 (2013) 1.
17. I. Kruk, P. Zajdel, W. van Beek, I. Bakaimi, A. Lappas, C. Stock, & M. A. Green, *J. Am. Chem. Soc.*, 133 (2011) 13950.
18. M. M. Doeff, T. J. Richardson, J. Hollingsworth, C. W. Yuan, and M. Gonzales, *J. Power Sources*, 112 (2002) 294.
19. F. Sauvage, E. Baudrin, and J. M. Tarascon, *Sensor Actuat. B-Chem.*, 120 (2007) 638.
20. F. Sauvage, L. Laffont, J. M. Tarascon, and E. Baudrin, *Inorg. Chem.*, 46 (2007) 3289.
21. J. A. Saint, M. M. Doeff, and J. Wilcox, *Chem. Mater.*, 20 (2008) 3404.
22. E. Hosono, H. Matsuda, I. Honma, S. Fujihara, M. Ichihara, and H. Zhou, *J. Power Sources*, 182 (2008) 349.
23. Y. Li, and Y. Wu, *Nano Res.*, 2 (2009) 54.
24. X. Zhou, R. K. Guduru, and P. Mohanty, *J. Mater. Chem. A*, 1 (2013) 2757.
25. L. Zhao, J. Ni, H. Wang, and L. Gao, *Funct. Mater. Lett.*, 6 (2013) 1.
26. P. Zhan, S. Wang, Y. Yuan, K. Jiao, and S. Jiao, *J. Electrochem. Soc.*, 162 (2015) A1028.
27. P. Le Goff, N. Baffier, S. Bach, and J. P. Pereira-Ramos, *Mater. Res. Bull.*, 31 (1996) 63.
28. B. Folch, J. Larionova, Y. Guari, C. Guérin, and C. Reibel, *J. Solid State Chem.*, 178 (2005) 2368.
29. Y. Park, S. W. Lee, K. H. Kim, B. K. Min, A. K. Nayak, D. Pradhan, and Y. Sohn, *Sci. Rep.*, 5 (2015) 1.
30. M. C. Biesinger, B. P. Payne, A. P. Grosvenor, L. W. Lau, A. R. Gerson, and R. S. C. Smart, *Appl. Surf. Sci.*, 257 (2011) 2717.

© 2016 The Authors. Published by ESG ([www.electrochemsci.org](http://www.electrochemsci.org)). This article is an open access article distributed under the terms and conditions of the Creative Commons Attribution license (<http://creativecommons.org/licenses/by/4.0/>).